Environmental Science & Technology

pubs.acs.org/est

Article

Transformation of Graphitic Carbon Nitride by Reactive Chlorine Species: "Weak" Oxidants Are the Main Players

Mengqiao Li, David P. Durkin, Gordon Waller, Yaochun Yu, Yujie Men, Tao Ye, Hanning Chen,* and Danmeng Shuai*

Cite This: https://doi.org/10.1021/acs.est.2c06381

Read Online

ACCESS | Metrics & More | Article Recommendations | Supporting Information

ABSTRACT: Graphitic carbon nitride (g-C_3N_4) nanomaterials hold great promise in diverse applications; however, their stability in engineering systems and transformation in nature are largely underexplored. We evaluated the stability, aging, and environmental impact of g-C_3N_4 nanosheets under the attack of free chlorine and reactive chlorine species (RCS), a widely used oxidant/disinfectant and a class of ubiquitous radical species, respectively. g-C_3N_4 nanosheets were slowly oxidized by free chlorine even at a high concentration of 200−1200 mg L^{-1}, but they decomposed rapidly when ClO· and/or $Cl_2^{\bullet-}$ were the key oxidants. Though $Cl_2^{\bullet-}$ and ClO· are considered weaker oxidants in previous studies due to their lower reduction potentials and slower reaction kinetics than ·OH and Cl·, our study highlighted that their electrophilic attack efficacy on g-C_3N_4 nanosheets was on par with ·OH and much higher than Cl·. A trace level of covalently bonded Cl (0.28−0.55 at%) was introduced to g-C_3N_4 nanosheets after free chlorine and RCS oxidation. Our study elucidates the environmental fate and transformation of g-C_3N_4 nanosheets, particularly under the oxidation of chlorine-containing species, and it also provides guidelines for designing reactive, robust, and safe nanomaterials for engineering applications.

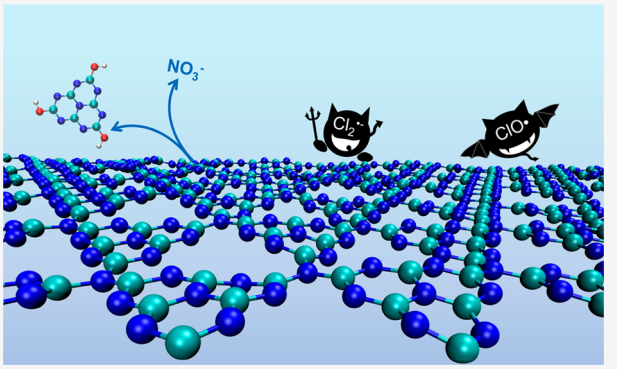

KEYWORDS: *graphitic carbon nitride, nanosheets, nanomaterial aging, reactive chlorine species, computational simulations*

INTRODUCTION

Reactive species are important for both engineering and natural systems. They play critical roles in chemical contaminant degradation, microbial inactivation, biogeochemical cycling, nanomaterial aging and transformation, etc.[1−6] For example, as the most powerful oxidant in water (E^0 = 2.8 eV), hydroxyl radicals (·OH) are commonly generated in advanced oxidation processes (AOPs) to remove persistent micropollutants.[7] ·OH are also ubiquitous in natural aquatic environments. They can be produced via the photolysis of nitrite, nitrate, and dissolved organic matter (DOM), photo-Fenton reactions, microbial activities, and overturn-induced aeration of anoxic bottom water.[8−11] Reactive chlorine species (RCS), like chlorine atoms (Cl·), chlorine oxide radicals (ClO·), and dichlorine radical anions ($Cl_2^{\bullet-}$), have attracted great attention for AOPs in recent years,[12−16] and they can be produced through ultraviolet light (UV)-activated photolysis of free chlorine and monochloramine.[17−20] Moreover, emerging technologies such as photocatalysis, electrocatalysis, and photoelectrocatalysis have been discovered to produce a high concentration of RCS for effective pollutant control.[21−26] Similar to ·OH, RCS are also ubiquitous in natural aquatic systems, especially in brines, estuaries, and seawater, and they are generated through the oxidation of chloride by ·OH, singlet oxygen ($^1O_2$), and photoexcited DOM.[29−32] When compared to ·OH, RCS oxidation could be less thermodynamically favorable due to their lower reduction potentials (the reduction potential of Cl·, $Cl_2^{\bullet-}$, and ClO· is 2.5, 2.2, and 1.5−1.8 eV, respectively).[15,16,30] Moreover, RCS is more selective than ·OH: Cl· launches the electrophilic attack on aromatic rings whereas $Cl_2^{\bullet-}$ and ClO· prefer to react with aromatics with electron-donating groups through electron transfer.[27−30] However, RCS-induced oxidation is likely to form halogenated byproducts, which may raise concerns for human health and ecosystems.[16,32−35]

Graphitic carbon nitride (g-C_3N_4) nanosheets are promising photoreactive engineered nanomaterials with interconnected *s*-triazines or heptazines units. They have found broad applications in catalysis, pollution control, membrane separation, chemical sensing, and beyond.[36−40] For example, g-C_3N_4 has been used to activate free chlorine and generate ·OH and

Received: September 1, 2022
Revised: January 24, 2023
Accepted: January 25, 2023

RCS for degrading persistent organic micropollutants in photocatalysis.[41] However, recent studies have discovered one significant limitation of g-C_3N_4 for engineering applications: g-C_3N_4 can decompose rapidly in an oxidative environment and loses its structural and chemical integrity. Though g-C_3N_4 was stable under the attack of O_3, H_2O_2, and $O_2^{-\bullet}$, ·OH could tear heptazine units apart from the g-C_3N_4 framework to release cyameluric acid and nitrate in an aqueous environment,[42] and the assistance of photoinduced holes (h^+) in photocatalysis further exacerbate the decomposition of g-C_3N_4 nanosheets.[43] Fast self-decomposition of g-C_3N_4 was also discovered in an inert gaseous environment with the presence of CO_2 or Ar in photocatalysis, and the chemical instability of g-C_3N_4 was attributed to the synergy of adsorbed hydroxyl groups and photoinduced charges.[44] Moreover, considering the global commercialization and extensive application of engineered nanomaterials like g-C_3N_4 nanosheets, incidental release and inappropriate disposal of these nanomaterials into nature are inevitable, which may pose serious and increasing environmental risks.[45−47] The transformation of nanomaterials in nature also determines their adverse impacts on human health and threats to ecosystems. RCS are important and abundant radicals in both engineering and natural systems, but their critical role in degrading and aging engineered nanomaterials like g-C_3N_4 nanosheets is unknown to date.

In this study, we investigated the transformation of g-C_3N_4 nanosheets under RCS attack by integrating reaction kinetic evaluations, advanced spectroscopic and microscopic characterizations, and molecular simulations. We prepared two g-C_3N_4 nanosheets, one with more defects, edges, and pores compared to the other and evaluated their degradation kinetics with the presence of free chlorine and RCS (i.e., chlorination and photocatalytic chlorination). Next, molecular simulations were conducted to understand the reaction mechanism of how free chlorine and RCS attack g-C_3N_4 nanosheets. Surprisingly, it was discovered that ClO· and/or $Cl_2^{\bullet-}$ rapidly degraded g-C_3N_4 nanosheets, though they are generally considered weak oxidants. This observation could be attributed to the feasible electrophilic attack of the nanosheets by ClO· and/or $Cl_2^{\bullet-}$ but not Cl·. Our work is novel because it provides the first insights into the fate, transformation, and reactivity of g-C_3N_4 nanosheets under RCS attack to understand their behavior in engineering and natural environments. Research outcomes provide guidelines for designing advanced engineered nanomaterials with improved robustness and reduced adverse environmental impacts for practice.

MATERIALS AND METHODS

Synthesis and Characterization of g-C_3N_4 Nanosheets. Two different g-C_3N_4 nanosheets were synthesized through thermal polycondensation of alcohol intercalated melamine-cyanuric acid supramolecules (denoted as D) and thermal exfoliation of bulk g-C_3N_4 powder (denoted as M2), respectively. Synthesis details are reported in our previous publication.[43] Chemicals for synthesis are listed in Text S1. Material characterization details, including CHNCl analysis, UV−vis diffuse reflectance spectroscopy, and X-ray photoelectron spectroscopy (XPS), can be found in Text S2.

g-C_3N_4 Nanosheet Aging. One hundred twenty milligrams of D or M2 was suspended in 120 mL of a 100 mM phosphate buffer (pH 7.5) in a 125 mL polytetrafluoroethylene/silicone lined glass septa jar. An appropriate amount (0.18−1.1 mL) of sodium hypochlorite solution (136 g L^{-1} of free chlorine) was added to the jar to reach free chlorine concentrations of 200, 500, and 1200 mg L^{-1}. A much higher concentration of free chlorine than that for disinfection was used because g-C_3N_4 nanosheets were relatively resistant to free chlorine oxidation and the photocatalytic chlorination treatment consumed free chlorine rapidly (details in results and discussion). The jar was kept in the dark or irradiated with a light-emitting diode (LED, 7 W, 395 nm) for chlorination and photocatalytic chlorination, respectively, and treatment systems are denoted as Cl_2-200/500/1200 and Photo-Cl_2-200/500/1200. As shown in Figure S1, the jar showed negligible absorption of the 395 nm photons generated by the LED light source. Under LED irradiation, g-C_3N_4 nanosheets were excited to produce photoinduced electrons (e^-) and h^+, and the e^- and h^+ reacted with free chlorine to produce RCS and then degraded g-C_3N_4 nanosheets (details in the Results and Discussion section). The concentration of free chlorine was determined with a drop count titration-based commercial test kit (HACH, model CN-65, 1−20 mg L^{-1}). All experiments were performed with at least three independent replicates.

After treatment, excessive sodium thiosulfate was added to quench residual oxidants, and aged g-C_3N_4 nanosheets were harvested by ultracentrifugation at 30,000 rpm (108,860*g*, Beckman JXN30). The supernatant of g-C_3N_4 nanosheets after (photocatalytic) chlorination and ultracentrifugation was filtered with a 0.2 μm polyvinylidene difluoride syringe filter for further analysis. The concentration of nitrate ions in the filtered supernatant was determined by ion chromatography (IC, Dionex ICS-1100; Dionex IonPac AS18 column) using 10 mM NaOH as the eluent and 0.25 mL min^{-1} as the flow rate. The concentration of released organic compounds was analyzed by a total organic carbon (TOC) analyzer. A gas chromatography−mass spectrometer (GC−MS) and an ultra-performance liquid chromatography−mass spectrometer (UPLC−MS) were used to detect the volatile and nonvolatile chlorinated oxidation byproducts. Details are provided in Text S5.

RCS Semiquantification and Presence/Absence Analysis. To quantify the generated reactive species (·OH, Cl·, ClO·, and $Cl_2^{\bullet-}$) in photocatalytic chlorination, nitrobenzene (NB), benzoic acid (BA), 1,4-dimethoxybenzene (DMOB), and CBZ were used as probe compounds (Text S3).[15,48,49] As shown in Table S1, NB only reacts with ·OH; BA reacts with both ·OH and Cl·; DMOB can be oxidized by ·OH, Cl·, and ClO·; while CBZ is vulnerable under the attack of these four radicals. A probe was spiked into g-C_3N_4 suspensions at the beginning of each reaction (∼10 min), and samples were collected continuously for up to 1 min. High-performance liquid chromatography (HPLC) was used to determine probe concentrations and degradation kinetics (Table S2). The radical concentrations were calculated for the initial stage of each treatment (details in Text S3). Specifically, probes were added independently for quantifying radical concentrations (Table S3). Control experiments of probe photocatalytic degradation were conducted in a 100 mM phosphate buffer (pH 7.5) with the presence of g-C_3N_4 nanosheets. DMOB and CBZ were susceptible to photocatalytic degradation, while the removal of NB and BA was negligible (Table S3). Therefore, negligible ·OH was present in g-C_3N_4-based photocatalysis when free chlorine was absent, and the contribution of direct photocatalysis should be deducted from the degradation kinetics of DMOB and CBZ when determining the concentration of ClO· and $Cl_2^{\bullet-}$ in photocatalytic chlorination

https://doi.org/10.1021/acs.est.2c06381
Environ. Sci. Technol. XXXX, XXX, XXX−XXX

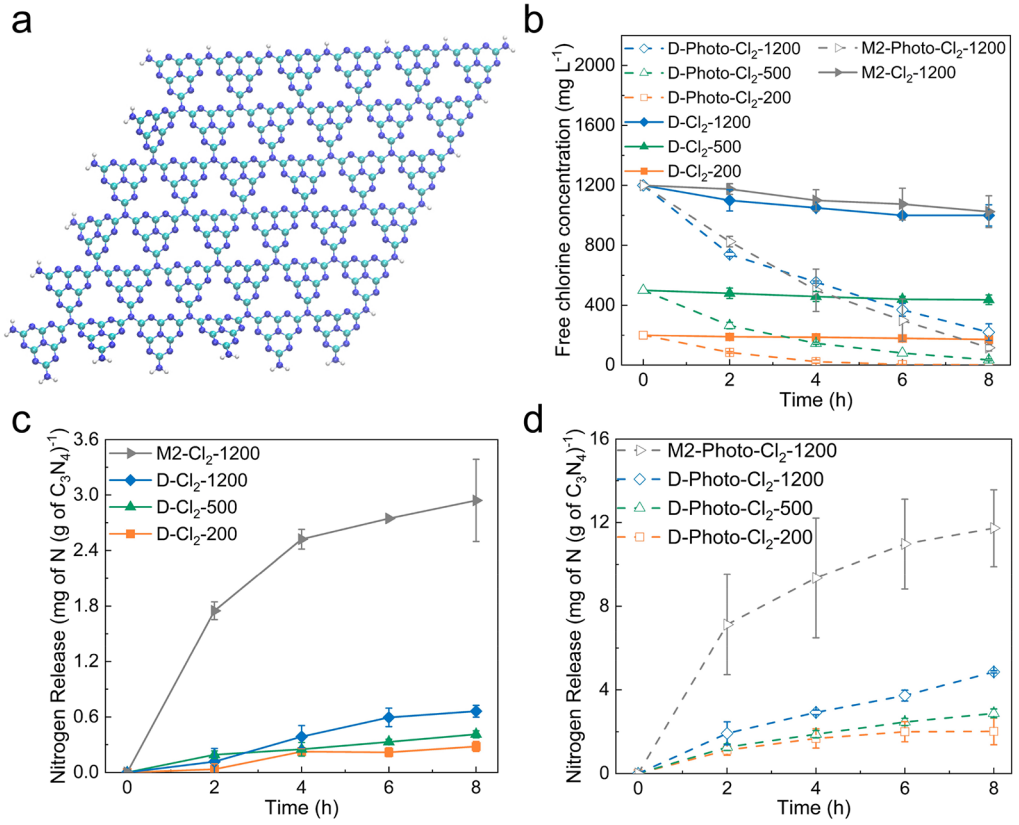

Figure 1. (a) Molecular structure of a g-C_3N_4 nanosheet terminated by amine groups. White, cyan, and blue balls in the structure refer to hydrogen, carbon, and nitrogen atoms, respectively. (b) Free chlorine concentration during the aging processes of D and M2. The nitrogen release as nitrate ions during the aging of D and M2 in the (c) dark or (d) under LED (7 W, 395 nm) irradiation. Cl_2-200/500/1200 and Photo-Cl_2-200/500/1200 represent chlorination and photocatalytic chlorination of g-C_3N_4 nanosheets with an initial spiked free chlorine concentration of 200, 500, or 1200 mg L^{-1}. Treatment conditions are as follows: g-C_3N_4 nanosheet loading of 1 g L^{-1}, 100 mM phosphate buffer (pH 7.5), initial spiked free chlorine concentration of 200, 500, or 1200 mg L^{-1} in the dark or under light irradiation. The error bars represent average ± standard deviation.

(Table S4). DMOB and CBZ were also amenable to direct oxidation by free chlorine (>100 mg L^{-1}, Table S3), which prevented the accurate quantification of RCS (Table S4). Fortunately, we were still able to use probe tests to validate the absence and presence of ·OH and RCS, by comparing the measured first-order reaction rate of probes in photocatalytic chlorination with that in control experiments of direct photocatalysis and direct free chlorine oxidation (details in Text S3).

Computational Simulation. As shown in Figure 1a, g-C_3N_4 nanosheets were modeled as a 6 × 6 heptazine supercell, which was connected by tertiary amine groups and terminated by primary and secondary amine groups. A three-dimensional simulation box as large as 120 Å × 100 Å × 120 Å with α = 90°, β = 60°, and γ = 90° was adopted to diminish artifacts due to periodic boundary conditions. Unless otherwise specified, all simulations were carried out by the open-source CP2K package[50] with the Goedecker–Teter–Hutter (GTH) pseudopotential,[51] Perdew–Burke–Ernzerhof (PBE) exchange-correlation function,[52] implicit solvation effect[53] with a dielectric constant of 78.4, and polarized-valence-double-ζ (PVDZ) basis set.[54] To reveal the electrophilic attack efficacy of ·OH, Cl·, ClO·, $Cl_2^{\bullet-}$, and OCl^- on g-C_3N_4 nanosheets, the interaction geometries between reactive species and the nanosheets were optimized in the initial (S_I), transition (S_T), and final (S_F) states before calculating the associated enthalpy changes ($\Delta H_{rxn} = E(S_F) - E(S_I)$) and activation energies ($\Delta E_{act} = E(S_T) - E(S_I)$). Specifically, the Broyden–Flectcher–Goldfarb–Shanno (BFGS) algorithm[55] was employed to locate S_I and S_F by minimizing their energies to local minima, whereas the climbing image nudged elastic band (CI-NEB) approach[56] was utilized to ascertain S_T with eight images sequentially connected by springs featuring a harmonic force constant of 0.5 hartree $Bohr^{-2}$.

RESULTS AND DISCUSSION

Chlorination of g-C_3N_4 Nanosheets. Two different g-C_3N_4 nanosheets, i.e., D and M2, were synthesized, and they have comparable lateral sizes.[43] However, D had a more well-defined structure than M2, and M2 has more pores, edges, and defects, as demonstrated in our previous study.[43] Therefore, the specific area of M2 (168 ± 1 m^2 g^{-1}) was 7.78 times larger than that of D (21.6 ± 3.4 m^2 g^{-1}).[43] More importantly, M2 has more active sites in photocatalysis and shows 2.33–2.70 times higher photocatalytic activity than D in degrading phenol under various light sources.[43] To effectively age g-C_3N_4 nanosheets, a high initial concentration of free chlorine ($HOCl/OCl^-$) was used (200, 500, and 1200 mg L^{-1}) for chlorination in the dark, and nitrogen release was monitored to reflect the extent of g-C_3N_4 decomposition. Nitrate but not nitrite was detected by IC. Although only a small portion of free chlorine was consumed (Figure 1b, solid lines), D was continuously degraded to release nitrate ions for up to 8 h (Figure 1c). When the free chlorine concentration increased from 200 to 1200 mg L^{-1} (Cl_2-200 versus Cl_2-1200), the

https://doi.org/10.1021/acs.est.2c06381
Environ. Sci. Technol. XXXX, XXX, XXX−XXX

nitrogen release amount throughout the 8h treatment disproportionally increased from 0.28 ± 0.05 to only 0.66 ± 0.06 mg of N (g of g-C_3N_4 nanosheets)$^{-1}$. We speculate that free chlorine only attacked the defects of g-C_3N_4 nanosheets on edges. Similar to ·OH oxidation, the limited number of edge defects resulted in the slow decomposition of g-C_3N_4 nanosheets.[43] In addition, M2 released 4.45 times more nitrate (2.94 ± 0.44 mg of N (g of g-C_3N_4 nanosheets)$^{-1}$) than D when it was treated with 1200 mg L^{-1} of free chlorine (Figure 1c), further proving that M2 with more pores, edges, and defects was prone to degradation.

Production of ClO· and/or $Cl_2^{\bullet-}$ in the Photocatalytic Chlorination of g-C_3N_4 Nanosheets. HOCl and OCl^- (pK_a = 7.5) could absorb UV light (<340 nm) and produce radical species efficiently.[57,58] Since the LED light source used in this study had a central emission wavelength of 395 nm (ranging 380−440 nm, Figure S1), the direct photolysis of free chlorine for producing radicals was negligible. g-C_3N_4 nanosheets, by contrast, can be activated and produce $O_2^{\bullet-}$ (R1) effectively.[43,44,60] $O_2^{\bullet-}$ subsequently reacts with HOCl to produce ·OH and Cl· (R2), and simultaneously, ClO^- can be activated by e^- to generate $O^{\bullet-}$ (R3), which is next protonated to form ·OH.[41,61] ·OH will be further scavenged by Cl^- and HOCl/OCl^- to form ClO·, $ClOH^{\bullet-}$, Cl·, and $Cl_2^{\bullet-}$ (Figure S2).

$$O_2 + e^- \rightarrow O_2^{\bullet-},\ k = 1.9 \times 10^{10}\ M^{-1}s^{-1} \quad (R1)$$

$$HOCl + O_2^{\bullet-} \rightarrow \cdot OH + Cl^- + O_2,\ k = 7.5 \times 10^6\ M^{-1}s^{-1} \quad (R2)$$

$$ClO^- + e^- \rightarrow O^{\bullet-} + Cl^-,\ k = 7.2 \times 10^9\ M^{-1}s^{-1} \quad (R3)$$

NB, BA, DMOB, and CBZ were used as probes to quantify ·OH, Cl·, ClO·, and $Cl_2^{\bullet-}$ concentrations (Text S3).[15,48,49] We first tested radical concentrations at low free chlorine dosages (4−20 mg L^{-1}), and ·OH and Cl· were only present when the free chlorine concentration was 4 and 10 mg L^{-1} (Figure S3). With the increase of the free chlorine dosage, less ·OH but more ClO· was observed, consistent with previous reports.[62,63] We next tested RCS concentrations at high free chlorine dosages beyond 100 mg L^{-1}, and ·OH and Cl· became negligible (Table S4). However, direct chlorine oxidation of DMOB and CBZ at high free chlorine dosages interfered with the quantification of ClO· and $Cl_2^{\bullet-}$ (Text S3 and Table S4). We found that the measured pseudo-first-order degradation rate constants of DMOB and CBZ in photocatalytic chlorination were larger than the sum of the degradation rate in direct photocatalysis (photocatalytic oxidation of probes by g-C_3N_4 nanosheets) and direct free chlorine oxidation (probe oxidation only by free chlorine), indicating that ClO· and/or $Cl_2^{\bullet-}$ played a key role in probe degradation (Table S4). Because ·OH and Cl· were missing from photocatalytic chlorination with a high free chlorine dosage (200, 500, or 1200 mg L^{-1}), ClO· was hence identified as an important RCS, whereas $Cl_2^{\bullet-}$ might be present in photocatalytic chlorination. In contrast, no RCS or ·OH was found in dark chlorination, and free chlorine (HOCl/OCl^-) was the dominant oxidant.[64−66]

RCS-Induced g-C_3N_4 Nanosheet Aging. In contrast to chlorination, free chlorine was rapidly consumed to produce ClO· and/or $Cl_2^{\bullet-}$ (Figure 1b, dash lines) in photocatalytic chlorination, and simultaneously, D was oxidized and degraded to release more nitrate (Figure 1d). When the initial free chlorine concentration was 200 mg L^{-1} (Photo-Cl_2-200), with the rapid consumption of free chlorine, the 2 h averaged nitrogen release rate (NRR) of D decreased from 0.56 to 0.28 and to 0.16 mg of N (g of g-C_3N_4 nanosheets)$^{-1}$ h^{-1} for 0−2, 2−4, and 4−6 h treatment. The 2 h averaged NRR was negligible for the photocatalytic chlorination of D in 6−8 h treatment, possibly due to the depletion of free chlorine and ClO· and/or $Cl_2^{\bullet-}$. Increasing the initial free chlorine concentration to 500 mg L^{-1} (Photo-Cl_2-500), the 2 h averaged NRR of D only slightly decreased after 6 h of treatment. As for the photocatalytic chlorination of D with 1200 mg L^{-1} initial free chlorine concentration (Photo-Cl_2-1200), the 2 h averaged NRR maintained well for 8 h of treatment, showing the importance of a relatively high free chlorine concentration in sustaining the production of ClO· and/or $Cl_2^{\bullet-}$. M2 had a much higher 8 h averaged NRR when compared to D: 1.5 ± 0.2 versus 0.61 ± 0.01 mg of N (g of g-C_3N_4 nanosheets)$^{-1}$ h^{-1} for Photo-Cl_2-1200 in 8 h of treatment (Figure 1d). This is because M2 had higher photoreactivity, enabled more e^-/h^+ generation, and promoted ClO· and/or $Cl_2^{\bullet-}$ production in photocatalytic chlorination. In addition, M2 had more pores, edges, and defects, which rendered higher susceptibility to oxidation.

Aging Products of g-C_3N_4 Nanosheets. We first evaluated small and soluble compounds that were released from g-C_3N_4 nanosheets during all treatments. In addition to nitrate, soluble organic compounds including cyameluric acid were released from D and M2 after aging (Text S5, Figure S4). Particularly, photocatalytic chlorination resulted in an increased release of soluble organic compounds than chlorination, which agreed with the nitrogen release results. The reactions of organic matter with free chlorine and RCS always raise concerns in producing chlorinated organic byproducts,[35,67,68] so we also evaluated the production of trichloromethane, monochloroacetic acid, dichloroacetic acid, and trichloroacetic acid in g-C_3N_4 nanosheet aging. All byproducts were below the detection limit (i.e., 0.08 mg L^{-1} for trichloromethane and 0.1 mg L^{-1} for haloacetic acids), indicating that g-C_3N_4 nanosheet aging by free chlorine and RCS was less likely to generate trihalomethanes and haloacetic acids.

We next investigated the morphological, physical, chemical, and optical properties of g-C_3N_4 nanosheets after aging. Bulk composition analysis (Table S5) indicated that Cl was introduced to both D and M2 after all aging treatments. XPS analysis also confirmed the introduction of chlorine onto the g-C_3N_4 nanosheet surface and indicated an increase of surface oxygen content (Table S6). More importantly, C−Cl bonds were observed on the surface of the treated g-C_3N_4 nanosheets (Tables S6 and S7, Figure S5). The atomic percentage of covalently bonded Cl at the surface ranged from 0.28 to 0.55 at % (i.e., ca. 71−78% of the XPS measured chlorine, with remaining chlorine existing as Cl^-) for treated g-C_3N_4 nanosheets. Surprisingly, although ClO· and/or $Cl_2^{\bullet-}$ induced much faster decomposition of g-C_3N_4 nanosheets than free chlorine, photocatalytic chlorination did not introduce more C−Cl or Cl^- than chlorination. No significant difference in Cl contents was found between D and M2 after the treatment (Tables S5−S7). These results were in contrast with our previous study, in which the synergistic attack of holes and hydroxyl radicals not only lead to faster degradation of g-C_3N_4 nanosheets but also introduced much more oxygen-containing groups compared with the attack launched by hydroxyl radicals

https://doi.org/10.1021/acs.est.2c06381
Environ. Sci. Technol. XXXX, XXX, XXX−XXX

only.[43] We speculate that ClO· and/or $Cl_2^{\bullet-}$ perform as catalysts to transfer electrons in decomposing g-C_3N_4 nanosheets, and they were less likely to be incorporated into the bulk framework. It might also indicate that only limited sites on g-C_3N_4 nanosheets were amenable to RCS attack, but further studies are needed. Moreover, an increase in the atomic percentage of surface oxygen was observed in aged g-C_3N_4 nanosheets based on XPS (from 3.6% before aging to 4.3−4.6% after aging, Table S6), but the result also did not bias between treatment conditions (chlorination versus photocatalytic chlorination). The band gap of D and M2 was marginally changed after photochlorination (Figure S6), but the introduction of Cl atoms and the increase of surface oxygen content (Tables S6 and S7) could tailor the electronic properties of g-C_3N_4 nanosheets and consequent photoreactivity.

Molecular Simulations for the Electrophilic Attack of g-C_3N_4 Nanosheets by Radicals and Free Chlorine. We first simulated the electrophilic attack of radicals and free chlorine on g-C_3N_4 nanosheets by assuming the nanosheets were electrically neutral. Free chlorine was abundant in all treatments. Based on our experimental analysis, RCS like ClO· and/or $Cl_2^{\bullet-}$ were produced in photocatalytic chlorination where g-C_3N_4 nanosheets were photoexcited to produce e^-/h^+ and possess localized charges. However, a localized h^+ on a heptazine unit of g-C_3N_4 nanosheets only has a lifetime of nanoseconds much shorter than the lifetime of a radical, so most heptazine units are not photoexcited or charged under light irradiation.[59] In addition, radicals produced on g-C_3N_4 nanosheets in photocatalytic chlorination can diffuse and react with heptazine units far away from where the radicals are originally generated. Therefore, it is reasonable to investigate the interaction of radicals and neutral g-C_3N_4 nanosheets. To reveal the efficacy of electrophilic attack on g-C_3N_4 nanosheets by free chlorine (represented by HOCl and OCl^-), ·OH, Cl·, ClO·, and $Cl_2^{\bullet-}$, the geometries of S_I, S_T, and S_F states of the reactive species interacting with the nanosheets were optimized. Then, the associated enthalpy changes and activation energies were evaluated as $\Delta H_{rxn} = E(S_F) - E(S_I)$ and $\Delta E_{act} = E(S_T) - E(S_I)$. Even though ·OH and Cl· were not found in our experimental setup, they were considered for simulations to compare the degradation mechanism of g-C_3N_4 nanosheets by diverse oxidants.

All electrophiles preferred attacking edge-site instead of bulk-phase heptazines. As shown in Figure S7a, the ·OH attack on a g-C_3N_4 nanosheet led to a short O−C bond of 1.41 Å, therefore affording a rather negative ΔH_{rxn} of −31.4 kcal mol^{-1} (Table 1). For such an exothermic electrophilic addition, its small ΔE_{act} of 1.2 kcal mol^{-1} is not surprising. When the less oxidative ClO· radical attacked a g-C_3N_4 nanosheet (Figure 2a), ΔH_{rxn} plunged to −4.0 kcal mol^{-1} for a weaker O−C bond with a longer length of 1.43 Å. As expected, the associated ΔE_{act} also increased to 4.9 kcal mol^{-1} due to the stabilized reactant of ClO· by resonance structures. For OCl^- (Figure S7b), the O−C bond remained at 1.43 Å for a similar ΔH_{rxn} of −6.4 kcal mol^{-1} while ΔE_{act} soared to 13.8 kcal mol^{-1} for the additional energy to break the O−H bond in the initial state. By contrast, the attack launched by HOCl (Figure S7c, Table 1) was thermodynamically unfavorable. Surprisingly, $Cl_2^{\bullet-}$ (Figure 2b) exhibited a nearly negligible ΔE_{act} of 0.1 kcal mol^{-1} that could be ascribed to the formation of a long and stable H−Cl−Cl−N chain connecting two edge-site heptazines (the right panel of Figure 2b). Interestingly, a three-atom chain

Table 1. Calculated Enthalpy Changes and Activation Energies for the Electrophilic Attack of ·OH, Cl·, ClO·, $Cl_2^{\bullet-}$, HOCl, and OCl^- on g-C_3N_4 Nanosheets with and without the Presence of a Photoinduced Hole (h^+)

reactive species	enthalpy change ΔH_{rxn} (kcal mol^{-1})	activation energy ΔE_{act} (kcal mol^{-1})
·OH	−31.4	1.2
ClO·	−4.0	4.9
OCl^-	−6.4	13.8
HOCl	+40.6	N/A
$Cl_2^{\bullet-}$	−10.1	0.1
Cl· (attack on carbon)	+6.4	N/A
Cl· (attack on nitrogen)	+8.1	N/A
·OH (h^+)	−8.9	3.1
ClO· (h^+)	+12.2	N/A
$Cl_2^{\bullet-}$ (h^+)	−16.1	0.6

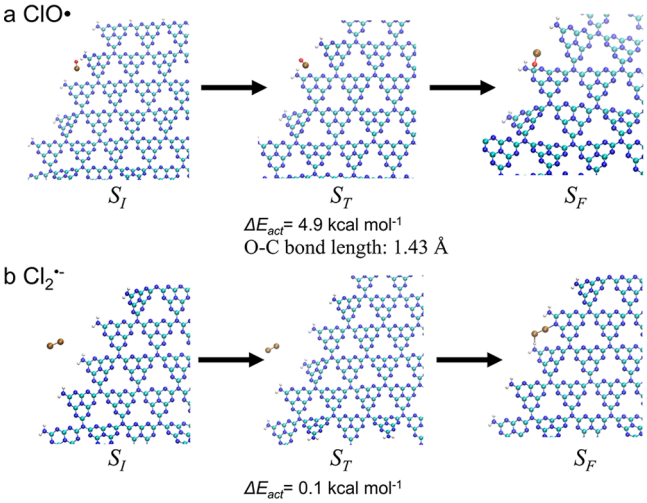

Figure 2. Optimized initial (S_I), transition (S_T), and final (S_F) states when a g-C_3N_4 nanosheet is attacked by (a) ClO· and (b) $Cl_2^{\bullet-}$. White, cyan, and blue balls in the structure refer to hydrogen, carbon, and nitrogen atoms, respectively. $\Delta E_{act} = E(S_T) - E(S_I)$.

such as H−Cl−N was not sufficiently long, excluding the possibility of forming an extra bridge between two heptazine units with a Cl·. Cl· could alternatively attack either a carbon (Figure S8a) or a nitrogen (Figure S8b) atom on the g-C_3N_4 nanosheet. Nevertheless, both attacking schemes resulted in positive ΔH_{rxn}, (i.e., ΔH_{rxn} = 6.4 kcal mol^{-1} for Cl· attack on carbon and ΔH_{rxn} = 8.1 kcal mol^{-1} for Cl· attack on nitrogen), making the addition of Cl· to a g-C_3N_4 nanosheet thermodynamically unfavorable.

We next evaluated the attack of RCS and free chlorine on a photoexcited g-C_3N_4 nanosheet in photocatalytic chlorination. The constrained density functional theory[69] was employed to impose a net charge of +1 on the edge-site heptazine that was being attacked by an electrophile. Particularly, we only explored the electrophiles whose ΔH_{rxn}s were negative and ΔE_{act}s were lower than 5.0 kcal mol^{-1} for a discernible reaction rate in the absence of light irradiation. For the ·OH-launched attack (Figure 3a), the O−C bond increased to 1.44 from 1.41 Å in S_F upon h^+ formation, resulting in a drastic escalation of ΔH_{rxn} from −31.4 to −8.9 kcal mol^{-1}. This 22.5 kcal mol^{-1} increase stemmed from the reduced electrophilicity of the

https://doi.org/10.1021/acs.est.2c06381
Environ. Sci. Technol. XXXX, XXX, XXX−XXX

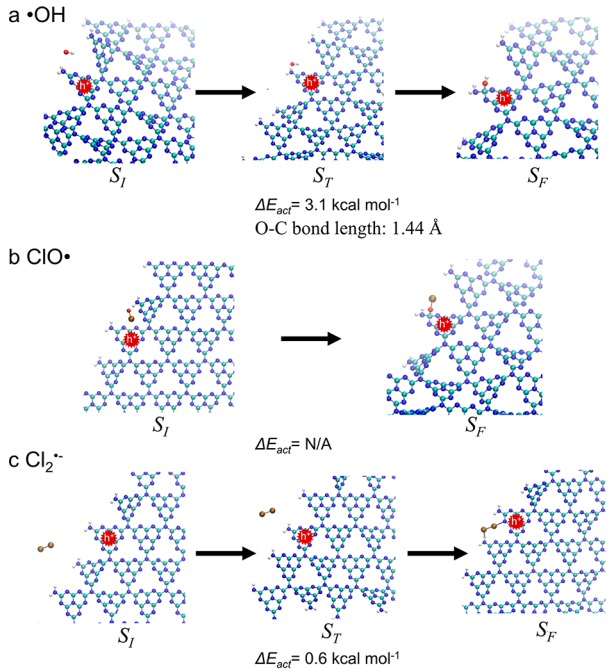

Figure 3. Optimized initial (S_I), transition (S_T), and final (S_F) states when the g-C_3N_4 nanosheet with a photoinduced hole (h^+) located at an edge-site heptazine is attacked by (a) ·OH, (b) ClO·, and (c) $Cl_2^{\bullet-}$. White, cyan, and blue balls in the structure refer to hydrogen, carbon, and nitrogen atoms, respectively. $\Delta E_{act} = E(S_T) - E(S_I)$.

ionized heptazine, which also increased ΔE_{act} from 1.2 to 3.1 kcal mol^{-1}. In fact, the reduced electrophilicity further flipped the sign of ΔH_{rxn} from negative to positive for ClO· (Table 1), making its attack on the g-C_3N_4 nanosheet nonspontaneous as shown in Figure 3b. On the other hand, the positively charged heptazine unit rendered a stronger electrostatic attraction to the anionic $Cl_2^{\bullet-}$ (Figure 3c), affording a rather negative ΔH_{rxn} of −16.1 kcal mol^{-1}, while still maintaining a small ΔE_{act} at 0.6 kcal mol^{-1}. Taken all together, the electrophilic attack efficacy of the explored oxidants is ordered as $Cl_2^{\bullet-}$ > ·OH > ClO· > OCl^- > Cl· > HOCl. $Cl_2^{\bullet-}$ and ClO·, which are conventionally believed as weak oxidants when compared to ·OH and Cl·, exhibit a powerful potential in decomposing g-C_3N_4 nanosheets.

Environmental Implication. Free chlorine is one of the most widely used disinfectants for water and wastewater disinfection, and it has attracted broad attention for AOPs in recent years because it can be excited under UV irradiation and through catalysis to produce highly reactive RCS for effective contaminant removal.[2,15,41,48,70] As a promising photoreactive material, g-C_3N_4 has been intensively investigated for photocatalytic oxidation and environmental remediation.[37,71,72] Some pioneering studies have validated the excellent performance of g-C_3N_4 for RCS production and contaminant degradation.[26,41] Therefore, it is likely that, in the near future, g-C_3N_4 will be used in engineering systems for water purification, and it can coexist with free chlorine and RCS. Our study revealed that g-C_3N_4 nanosheets were mildly oxidized in free chlorine, but they lost structural integrity and decomposed rapidly under the attack of ClO· and/or $Cl_2^{\bullet-}$, which calls for urgent attention to the material stability and robustness for long-term engineering applications. Our aging tests for g-C_3N_4 nanosheets were conducted with a high free chlorine concentration where ·OH was absent. Photocatalysis in a low dosage of free chlorine (<10 mg L^{-1}) better simulated the engineering practice in water and wastewater treatment, and it also introduced ·OH in addition to RCS, further exacerbating g-C_3N_4 nanosheets decomposition.[43] In addition, treating g-C_3N_4 with free chlorine can remove defects, introduce covalently bonded chlorine atoms, and alter the physiochemical properties, which could find broad applications for improving material photoreactivity.

RCS are also abundant in natural aquatic environments, especially saline water, and they play a critical role in the chemical transformation of (nano)materials. Incidentally released and inappropriately disposed of g-C_3N_4 can undergo RCS-induced transformation in natural aquatic environments and release byproducts like nitrate and cyameluric acid. Though g-C_3N_4 aging was not found to release small chlorinated organic molecules in our study, a thorough study should be conducted by leveraging high-resolution mass spectrometry to understand the formation of halogenated byproducts. Covalently bonded Cl was introduced to the g-C_3N_4 framework after chlorination and photocatalytic chlorination in our study, and thus, g-C_3N_4 oxidation by free chlorine and/or RCS could tailor the cytotoxicity, genotoxicity, and developmental toxicity of the material because of organic halogen formation.[73−75] Future studies should focus on a thorough and systematic toxicity evaluation of transformed g-C_3N_4, including toxicity to humans and ecosystems, based on which the rational design and synthesis of nanomaterials with higher safety standards may be realized. On the other hand, interdisciplinary collaborations are highly needed to provide reliable and realistic risk assessment of g-C_3N_4 and other photoreactive nanomaterials in an aquatic environment. For example, advanced analytic methods along with standardized sample pretreatment protocols should be developed to quantify the environmental concentrations of nanomaterials. Systematic experiment-oriented studies regarding the environmental transformation, behavior, and toxicity of photoreactive nanomaterials can be conducted to collect sufficient quality-assured data while robust statistical algorithms should be developed to create predictive models for the evaluation of upcoming nanomaterials.

■ ASSOCIATED CONTENT

Supporting Information

The Supporting Information is available free of charge at https://pubs.acs.org/doi/10.1021/acs.est.2c06381.

Discussions of chemicals and reagents, characterization of g-C_3N_4 nanosheets, reactive chlorine species semi-quantification and presence/absence analysis, and detection and quantification of released organics from g-C_3N_4 nanosheets in aging, tables of second-order reaction rate constants of probes used for detecting radical concentrations, parameters used in high performance liquid chromatography, probe degradation kinetics under direct photocatalysis and direct free chlorine oxidation, presence/absence of radicals in various systems, bulk elemental composition of g-C_3N_4 nanosheets after treatment, and X-ray photoelectron spectroscopy of fresh and aged g-C_3N_4 nanosheets, and figures of spectra of the LED lamp, radical chemistry of ·OH and reactive chlorine species in photocatalytic chlorination, initial radical distribution in photocatalytic chlorination with low free chlorine dosages, total organic

https://doi.org/10.1021/acs.est.2c06381
Environ. Sci. Technol. XXXX, XXX, XXX−XXX

carbon in the supernatant, X-ray photoelectron spectroscopy, UV−vis absorption spectra, and optimized initial (S_I), transition (S_T), and final (S_F) states (PDF)

AUTHOR INFORMATION

Corresponding Authors

Hanning Chen − *Texas Advanced Computing Center, the University of Texas at Austin, Austin, Texas 78758, United States;* orcid.org/0000-0003-3568-8039; Phone: 512-475-9411; Email: hanning.chen@austin.utexas.edu; Fax: 512-475-9445

Danmeng Shuai − *Department of Civil and Environmental Engineering, The George Washington University, Washington, D.C. 20052, United States;* orcid.org/0000-0003-3817-4092; Phone: 202-994-0506; Email: danmengshuai@gwu.edu; Fax: 202-994-0127; http://materwatersus.weebly.com/

Authors

Mengqiao Li − *Department of Civil and Environmental Engineering, The George Washington University, Washington, D.C. 20052, United States;* orcid.org/0000-0002-0567-9716

David P. Durkin − *Department of Chemistry, United States Naval Academy, Annapolis, Maryland 21402, United States;* orcid.org/0000-0001-5979-8449

Gordon Waller − *Chemistry Division, United States Naval Research Laboratory, Washington, D.C. 20375, United States*

Yaochun Yu − *Department of Chemical and Environmental Engineering, University of California, Riverside, Riverside, California 92521, United States; Department of Civil and Environmental Engineering, University of Illinois at Urbana−Champaign, Urbana, Illinois 61801, United States;* Present Address: Department of Environmental Chemistry, Swiss Federal Institute of Aquatic Science and Technology (Eawag), Dübendorf 8600, CH; orcid.org/0000-0001-9231-6026

Yujie Men − *Department of Chemical and Environmental Engineering, University of California, Riverside, Riverside, California 92521, United States; Department of Civil and Environmental Engineering, University of Illinois at Urbana−Champaign, Urbana, Illinois 61801, United States;* orcid.org/0000-0001-9811-3828

Tao Ye − *Department of Civil and Environmental Engineering, South Dakota School of Mines & Technology, Rapid City, South Dakota 57701, United States*

Complete contact information is available at: https://pubs.acs.org/10.1021/acs.est.2c06381

Notes

The authors declare no competing financial interest.

ACKNOWLEDGMENTS

The authors acknowledge NSF Grants CHE-1807617 for supporting our study. The authors also acknowledge the Air Force Office of Scientific Research (MIPR# F4FGA08354G001) and the United States Naval Academy Chemistry Department for facility support. G.W. was supported by the Office of Naval Research through the Naval Research Laboratory base program. Computational resources were provided by the Argonne Leadership Computing Facilities at Argonne National Laboratory under Department of Energy contract DE-AC-06CH11357 and by the Extreme Science and Engineering Discovery Environment at Texas Advanced Computing Center under National Science Foundation contract TG-CHE130008. The authors thank Elizabeth Eves and Dr. Julio A. N. T. Soares at the University of Illinois at Urbana−Champaign for CHNCl and band gap analyses and Jody Smiley and Dr. Zhiwu Wang at Virginia Tech for the TOC analysis. Any opinions, findings and conclusions, or recommendations expressed in this study are those of the authors and do not reflect the views of the U.S. Air Force or the U.S. Navy.

REFERENCES

(1) Kim, M. S.; Lee, C.; Kim, J.-H. Occurrence of Unknown Reactive Species in UV/H_2O_2 System Leading to False Interpretation of Hydroxyl Radical Probe Reactions. *Water Res.* **2021**, *201*, 117338.

(2) Li, X.; Kan, M.; Wang, T.; Qin, Z.; Zhang, T.; Qian, X.; Kuwahara, Y.; Mori, K.; Yamashita, H.; Zhao, Y. The ClO· Generation and Chlorate Suppression in Photoelectrochemical Reactive Chlorine Species Systems on $BiVO_4$ Photoanodes. *Appl. Catal., B* **2021**, *296*, 120387.

(3) Guo, Y.; Zhang, Y.; Yu, G.; Wang, Y. Revisiting the Role of Reactive Oxygen Species for Pollutant Abatement during Catalytic Ozonation: The Probe Approach versus the Scavenger Approach. *Appl. Catal., B* **2021**, *280*, 119418.

(4) Parker, K. M.; Mitch, W. A. Halogen Radicals Contribute to Photooxidation in Coastal and Estuarine Waters. *Proc. Natl. Acad. Sci. U.S.A.* **2016**, *113* (21), 5868−5873.

(5) Guo, K.; Zheng, S.; Zhang, X.; Zhao, L.; Ji, S.; Chen, C.; Wu, Z.; Wang, D.; Fang, J. Roles of Bromine Radicals and Hydroxyl Radicals in the Degradation of Micropollutants by the UV/Bromine Process. *Environ. Sci. Technol.* **2020**, *54* (10), 6415−6426.

(6) Qu, X.; Alvarez, P. J. J.; Li, Q. Photochemical Transformation of Carboxylated Multiwalled Carbon Nanotubes: Role of Reactive Oxygen Species. *Environ. Sci. Technol.* **2013**, *47* (24), 14080−14088.

(7) Oturan, M. A.; Aaron, J.-J. Advanced Oxidation Processes in Water/Wastewater Treatment: Principles and Applications. A Review. *Crit. Rev. Environ. Sci. Technol.* **2014**, *44* (23), 2577−2641.

(8) Minero, C.; Chiron, S.; Falletti, G.; Maurino, V.; Pelizzetti, E.; Ajassa, R.; Carlotti, M. E.; Vione, D. Photochemincal Processes Involving Nitrite in Surface Water Samples. *Aquat. Sci.* **2007**, *69* (1), 71−85.

(9) Minella, M.; De Laurentiis, E.; Maurino, V.; Minero, C.; Vione, D. Dark Production of Hydroxyl Radicals by Aeration of Anoxic Lake Water. *Sci. Total Environ.* **2015**, *527*−*528*, 322−327.

(10) Liao, P.; Yu, K.; Lu, Y.; Wang, P.; Liang, Y.; Shi, Z. Extensive Dark Production of Hydroxyl Radicals from Oxygenation of Polluted River Sediments. *Chem. Eng. J.* **2019**, *368*, 700−709.

(11) Page, S. E.; Kling, G. W.; Sander, M.; Harrold, K. H.; Logan, J. R.; McNeill, K.; Cory, R. M. Dark Formation of Hydroxyl Radical in Arctic Soil and Surface Waters. *Environ. Sci. Technol.* **2013**, *47* (22), 12860−12867.

(12) Bulman, D. M.; Mezyk, S. P.; Remucal, C. K. The Impact of PH and Irradiation Wavelength on the Production of Reactive Oxidants during Chlorine Photolysis. *Environ. Sci. Technol.* **2019**, *53* (8), 4450−4459.

(13) Guo, K.; Wu, Z.; Shang, C.; Yao, B.; Hou, S.; Yang, X.; Song, W.; Fang, J. Radical Chemistry and Structural Relationships of PPCP Degradation by UV/Chlorine Treatment in Simulated Drinking Water. *Environ. Sci. Technol.* **2017**, *51* (18), 10431−10439.

(14) Li, S.; Ao, X.; Li, C.; Lu, Z.; Cao, W.; Wu, F.; Liu, S.; Sun, W. Insight into PPCP Degradation by UV/NH_2Cl and Comparison with UV/NaClO: Kinetics, Reaction Mechanism, and DBP Formation. *Water Res.* **2020**, *182*, 115967.

(15) Zheng, W.; Zhu, L.; Liang, S.; Ye, J.; Yang, X.; Lei, Z.; Yan, Z.; Li, Y.; Wei, C.; Feng, C. Discovering the Importance of $ClO^{\bullet}$ in a Coupled Electrochemical System for the Simultaneous Removal of

https://doi.org/10.1021/acs.est.2c06381
Environ. Sci. Technol. XXXX, XXX, XXX−XXX

Carbon and Nitrogen from Secondary Coking Wastewater Effluent. *Environ. Sci. Technol.* **2020**, *54* (14), 9015−9024.
(16) Zhang, K.; Parker, K. M. Halogen Radical Oxidants in Natural and Engineered Aquatic Systems. *Environ. Sci. Technol.* **2018**, *52* (17), 9579−9594.
(17) Fang, J.; Fu, Y.; Shang, C. The Roles of Reactive Species in Micropollutant Degradation in the UV/Free Chlorine System. *Environ. Sci. Technol.* **2014**, *48* (3), 1859−1868.
(18) Xiang, Y.; Fang, J.; Shang, C. Kinetics and Pathways of Ibuprofen Degradation by the UV/Chlorine Advanced Oxidation Process. *Water Res.* **2016**, *90*, 301−308.
(19) Bu, L.; Zhou, S.; Zhu, S.; Wu, Y.; Duan, X.; Shi, Z.; Dionysiou, D. D. Insight into Carbamazepine Degradation by UV/Monochloramine: Reaction Mechanism, Oxidation Products, and DBPs Formation. *Water Res.* **2018**, *146*, 288−297.
(20) Chuang, Y.-H.; Chen, S.; Chinn, C. J.; Mitch, W. A. Comparing the UV/Monochloramine and UV/Free Chlorine Advanced Oxidation Processes (AOPs) to the UV/Hydrogen Peroxide AOP Under Scenarios Relevant to Potable Reuse. *Environ. Sci. Technol.* **2017**, *51* (23), 13859−13868.
(21) Jothinathan, L.; Hu, J. Kinetic Evaluation of Graphene Oxide Based Heterogenous Catalytic Ozonation for the Removal of Ibuprofen. *Water Res.* **2018**, *134*, 63−73.
(22) Li, Y.; Ouyang, S.; Xu, H.; Wang, X.; Bi, Y.; Zhang, Y.; Ye, J. Constructing Solid-Gas-Interfacial Fenton Reaction over Alkalinized-C_3N_4 Photocatalyst To Achieve Apparent Quantum Yield of 49% at 420 Nm. *J. Am. Chem. Soc.* **2016**, *138* (40), 13289−13297.
(23) Zhang, Y.; Li, J.; Bai, J.; Li, X.; Shen, Z.; Xia, L.; Chen, S.; Xu, Q.; Zhou, B. Total Organic Carbon and Total Nitrogen Removal and Simultaneous Electricity Generation for Nitrogen-Containing Wastewater Based on the Catalytic Reactions of Hydroxyl and Chlorine Radicals. *Appl. Catal., B* **2018**, *238*, 168−176.
(24) Chung, C. M.; Hong, S. W.; Cho, K.; Hoffmann, M. R. Degradation of Organic Compounds in Wastewater Matrix by Electrochemically Generated Reactive Chlorine Species: Kinetics and Selectivity. *Catal. Today* **2018**, *313*, 189−195.
(25) Li, F.; Sun, L.; Liu, Y.; Fang, X.; Shen, C.; Huang, M.; Wang, Z.; Dionysiou, D. D. A $ClO^{\bullet-}$ Mediated Photoelectrochemical Filtration System for Highly-Efficient and Complete Ammonia Conversion. *J. Hazard. Mater.* **2020**, *400*, 123246.
(26) Guo, Q.; Song, H.; Sun, M.; Yuan, X.; Su, Y.; Lv, Y. Co_3O_4 Modified Polymeric Carbon Nitride for External Light-Free Chlorine Activating Degradation of Organic Pollutants. *J. Hazard. Mater.* **2022**, *429*, 128193.
(27) Parker, K. M.; Pignatello, J. J.; Mitch, W. A. Influence of Ionic Strength on Triplet-State Natural Organic Matter Loss by Energy Transfer and Electron Transfer Pathways. *Environ. Sci. Technol.* **2013**, *47* (19), 10987−10994.
(28) Yang, Y.; Pignatello, J. Participation of the Halogens in Photochemical Reactions in Natural and Treated Waters. *Molecules* **2017**, *22* (10), 1684.
(29) Méndez-Díaz, J. D.; Shimabuku, K. K.; Ma, J.; Enumah, Z. O.; Pignatello, J. J.; Mitch, W. A.; Dodd, M. C. Sunlight-Driven Photochemical Halogenation of Dissolved Organic Matter in Seawater: A Natural Abiotic Source of Organobromine and Organoiodine. *Environ. Sci. Technol.* **2014**, *48* (13), 7418−7427.
(30) Sharma, V. K. Use of Iron(VI) and Iron(V) in Water and Wastewater Treatment. *Water Sci. Technol.* **2004**, *49* (4), 69−74.
(31) Lei, Y.; Cheng, S.; Luo, N.; Yang, X.; An, T. Rate Constants and Mechanisms of the Reactions of $Cl^{\bullet}$ and $Cl_2^{\bullet-}$ with Trace Organic Contaminants. *Environ. Sci. Technol.* **2019**, *53* (19), 11170−11182.
(32) Lei, Y.; Lei, X.; Westerhoff, P.; Zhang, X.; Yang, X. Reactivity of Chlorine Radicals ($Cl^{\bullet}$ and $Cl_2^{\bullet-}$) with Dissolved Organic Matter and the Formation of Chlorinated Byproducts. *Environ. Sci. Technol.* **2021**, *55* (1), 689−699.
(33) Leri, A. C.; Mayer, L. M.; Thornton, K. R.; Northrup, P. A.; Dunigan, M. R.; Ness, K. J.; Gellis, A. B. A Marine Sink for Chlorine in Natural Organic Matter. *Nat. Geosci.* **2015**, *8* (8), 620−624.
(34) Winder, C. The Toxicology of Chlorine. *Environ. Res.* **2001**, *85* (2), 105−114.
(35) Bulman, D. M.; Remucal, C. K. Role of Reactive Halogen Species in Disinfection Byproduct Formation during Chlorine Photolysis. *Environ. Sci. Technol.* **2020**, *54* (15), 9629−9639.
(36) Han, E.-X.; Li, Y.-Y.; Wang, Q.-H.; Huang, W.-Q.; Luo, L.; Hu, W.; Huang, G.-F. Chlorine Doped Graphitic Carbon Nitride Nanorings as an Efficient Photoresponsive Catalyst for Water Oxidation and Organic Decomposition. *J. Mater. Sci. Technol.* **2019**, *35* (10), 2288−2296.
(37) Su, F.; Mathew, S. C.; Lipner, G.; Fu, X.; Antonietti, M.; Blechert, S.; Wang, X. Mpg-C_3N_4-Catalyzed Selective Oxidation of Alcohols Using O_2 and Visible Light. *J. Am. Chem. Soc.* **2010**, *132* (46), 16299−16301.
(38) Dong, G.; Zhang, Y.; Pan, Q.; Qiu, J. A Fantastic Graphitic Carbon Nitride (g-C_3N_4) Material: Electronic Structure, Photocatalytic and Photoelectronic Properties. *J. Photochem. Photobiol.* **2014**, *20*, 33−50.
(39) Liras, M.; Barawi, M.; de la Peña O'Shea, V. A. Hybrid Materials Based on Conjugated Polymers and Inorganic Semiconductors as Photocatalysts: From Environmental to Energy Applications. *Chem. Soc. Rev.* **2019**, *48* (22), 5454−5487.
(40) Liu, J.; Wang, H.; Antonietti, M. Graphitic Carbon Nitride "Reloaded": Emerging Applications beyond (Photo)Catalysis. *Chem. Soc. Rev.* **2016**, *45* (8), 2308−2326.
(41) Cheng, Z.; Ling, L.; Wu, Z.; Fang, J.; Westerhoff, P.; Shang, C. Novel Visible Light-Driven Photocatalytic Chlorine Activation Process for Carbamazepine Degradation in Drinking Water. *Environ. Sci. Technol.* **2020**, *54* (18), 11584−11593.
(42) Xiao, J.; Han, Q.; Xie, Y.; Yang, J.; Su, Q.; Chen, Y.; Cao, H. Is C_3N_4 Chemically Stable toward Reactive Oxygen Species in Sunlight-Driven Water Treatment? *Environ. Sci. Technol.* **2017**, *51* (22), 13380−13387.
(43) Li, M.; Liu, D.; Chen, X.; Yin, Z.; Shen, H.; Aiello, A.; McKenzie, K. R.; Jiang, N.; Li, X.; Wagner, M. J.; Durkin, D. P.; Chen, H.; Shuai, D. Radical-Driven Decomposition of Graphitic Carbon Nitride Nanosheets: Light Exposure Matters. *Environ. Sci. Technol.* **2021**, *55* (18), 12414−12423.
(44) Chen, P.; Dong, X.; Huang, M.; Li, K.; Xiao, L.; Sheng, J.; Chen, S.; Zhou, Y.; Dong, F. Rapid Self-Decomposition of g-C_3N_4 During Gas-Solid Photocatalytic CO_2 Reduction and Its Effects on Performance Assessment. *ACS Catal.* **2022**, *12* (8), 4560−4570.
(45) Lead, J. R.; Batley, G. E.; Alvarez, P. J. J.; Croteau, M.-N.; Handy, R. D.; McLaughlin, M. J.; Judy, J. D.; Schirmer, K. Nanomaterials in the Environment: Behavior, Fate, Bioavailability, and Effects-An Updated Review. *Environ. Toxicol. Chem.* **2018**, *37* (8), 2029−2063.
(46) Schultz, C. L.; Adams, J.; Jurkschat, K.; Lofts, S.; Spurgeon, D. J. Chemical Transformation and Surface Functionalisation Affect the Potential to Group Nanoparticles for Risk Assessment. *Environ. Sci.: Nano* **2020**, *7* (10), 3100−3107.
(47) Lehutso, R. F.; Tancu, Y.; Maity, A.; Thwala, M. Aquatic Toxicity of Transformed and Product-Released Engineered Nanomaterials: An Overview of the Current State of Knowledge. *Process Saf. Environ. Prot.* **2020**, *138*, 39−56.
(48) Wang, W.-L.; Wu, Q.-Y.; Huang, N.; Wang, T.; Hu, H.-Y. Synergistic Effect between UV and Chlorine (UV/Chlorine) on the Degradation of Carbamazepine: Influence Factors and Radical Species. *Water Res.* **2016**, *98*, 190−198.
(49) Wu, Z.; Guo, K.; Fang, J.; Yang, X.; Xiao, H.; Hou, S.; Kong, X.; Shang, C.; Yang, X.; Meng, F.; Chen, L. Factors Affecting the Roles of Reactive Species in the Degradation of Micropollutants by the UV/Chlorine Process. *Water Res.* **2017**, *126*, 351−360.
(50) VandeVondele, J.; Krack, M.; Mohamed, F.; Parrinello, M.; Chassaing, T.; Hutter, J. Quickstep: Fast and Accurate Density Functional Calculations Using a Mixed Gaussian and Plane Waves Approach. *Comput. Phys. Commun.* **2005**, *167* (2), 103−128.
(51) Goedecker, S.; Teter, M.; Hutter, J. Separable Dual-Space Gaussian Pseudopotentials. *Phys. Rev. B* **1996**, *54* (3), 1703−1710.

https://doi.org/10.1021/acs.est.2c06381
Environ. Sci. Technol. XXXX, XXX, XXX−XXX

(52) Perdew, J. P.; Ernzerhof, M.; Burke, K. Rationale for Mixing Exact Exchange with Density Functional Approximations. *J. Chem. Phys.* **1996**, *105* (22), 9982−9985.
(53) Bani-Hashemian, M. H.; Brück, S.; Luisier, M.; VandeVondele, J. A Generalized Poisson Solver for First-Principles Device Simulations. *J. Chem. Phys.* **2016**, *144* (4), 044113.
(54) Woon, D. E.; Dunning, T. H. Gaussian Basis Sets for Use in Correlated Molecular Calculations. IV. Calculation of Static Electrical Response Properties. *J. Chem. Phys.* **1994**, *100* (4), 2975−2988.
(55) Broyden, C. G. The Convergence of a Class of Double-Rank Minimization Algorithms 1. General Considerations. *IMA J. Appl. Math* **1970**, *6* (1), 76−90.
(56) Henkelman, G.; Uberuaga, B. P.; Jónsson, H. A Climbing Image Nudged Elastic Band Method for Finding Saddle Points and Minimum Energy Paths. *J. Chem. Phys.* **2000**, *113* (22), 9901−9904.
(57) Yin, R.; Ling, L.; Shang, C. Wavelength-Dependent Chlorine Photolysis and Subsequent Radical Production Using UV-LEDs as Light Sources. *Water Res.* **2018**, *142*, 452−458.
(58) Guo, K.; Wu, Z.; Chen, C.; Fang, J. UV/Chlorine Process: An Efficient Advanced Oxidation Process with Multiple Radicals and Functions in Water Treatment. *Acc. Chem. Res.* **2022**, *55* (3), 286−297.
(59) Xiao, Y.; Tian, G.; Li, W.; Xie, Y.; Jiang, B.; Tian, C.; Zhao, D.; Fu, H. Molecule Self-Assembly Synthesis of Porous Few-Layer Carbon Nitride for Highly Efficient Photoredox Catalysis. *J. Am. Chem. Soc.* **2019**, *141* (6), 2508−2515.
(60) Li, Y.; Jin, R.; Xing, Y.; Li, J.; Song, S.; Liu, X.; Li, M.; Jin, R. Macroscopic Foam-Like Holey Ultrathin g-C_3N_4 Nanosheets for Drastic Improvement of Visible-Light Photocatalytic Activity. *Adv. Energy Mater.* **2016**, *6* (24), 1601273.
(61) Grebel, J. E.; Pignatello, J. J.; Mitch, W. A. Effect of Halide Ions and Carbonates on Organic Contaminant Degradation by Hydroxyl Radical-Based Advanced Oxidation Processes in Saline Waters. *Environ. Sci. Technol.* **2010**, *44* (17), 6822−6828.
(62) Kong, X.; Wu, Z.; Ren, Z.; Guo, K.; Hou, S.; Hua, Z.; Li, X.; Fang, J. Degradation of Lipid Regulators by the UV/Chlorine Process: Radical Mechanisms, Chlorine Oxide Radical $(ClO\bullet)^{-}$ Mediated Transformation Pathways and Toxicity Changes. *Water Res.* **2018**, *137*, 242−250.
(63) Kong, Q.; Lei, X.; Zhang, X.; Cheng, S.; Xu, C.; Yang, B.; Yang, X. The Role of Chlorine Oxide Radical (ClO•) in the Degradation of Polychoro-1,3-Butadienes in UV/Chlorine Treatment: Kinetics and Mechanisms. *Water Res.* **2020**, *183*, 116056.
(64) Deborde, M.; von Gunten, U. Reactions of Chlorine with Inorganic and Organic Compounds during Water Treatment—Kinetics and Mechanisms: A Critical Review. *Water Res.* **2008**, *42* (1−2), 13−51.
(65) Wang, W.-L.; Wu, Q.-Y.; Du, Y.; Huang, N.; Hu, H.-Y. Elimination of Chlorine-Refractory Carbamazepine by Breakpoint Chlorination: Reactive Species and Oxidation Byproducts. *Water Res.* **2018**, *129*, 115−122.
(66) Lau, S. S.; Abraham, S. M.; Roberts, A. L. Chlorination Revisited: Does Cl^{-} Serve as a Catalyst in the Chlorination of Phenols? *Environ. Sci. Technol.* **2016**, *50* (24), 13291−13298.
(67) Ding, S.; Deng, Y.; Bond, T.; Fang, C.; Cao, Z.; Chu, W. Disinfection Byproduct Formation during Drinking Water Treatment and Distribution: A Review of Unintended Effects of Engineering Agents and Materials. *Water Res.* **2019**, *160*, 313−329.
(68) How, Z. T.; Linge, K. L.; Busetti, F.; Joll, C. A. Organic Chloramines in Drinking Water: An Assessment of Formation, Stability, Reactivity and Risk. *Water Res.* **2016**, *93*, 65−73.
(69) Wu, Q.; Van Voorhis, T. Constrained Density Functional Theory and Its Application in Long-Range Electron Transfer. *J. Chem. Theory Comput.* **2006**, *2* (3), 765−774.
(70) Wang, X.; Sun, M.; Zhao, Y.; Wang, C.; Ma, W.; Wong, M. S.; Elimelech, M. In Situ Electrochemical Generation of Reactive Chlorine Species for Efficient Ultrafiltration Membrane Self-Cleaning. *Environ. Sci. Technol.* **2020**, *54* (11), 6997−7007.
(71) Zhao, X.; Pan, D.; Chen, X.; Li, R.; Jiang, T.; Wang, W.; Li, G.; Leung, D. Y. C. G-C_3N_4 Photoanode for Photoelectrocatalytic Synergistic Pollutant Degradation and Hydrogen Evolution. *Appl. Surf. Sci.* **2019**, *467*−*468*, 658−665.
(72) Jiang, W.; Luo, W.; Wang, J.; Zhang, M.; Zhu, Y. Enhancement of Catalytic Activity and Oxidative Ability for Graphitic Carbon Nitride. *J. Photochem. Photobiol. C* **2016**, *28*, 87−115.
(73) Han, J.; Zhang, X.; Jiang, J.; Li, W. How Much of the Total Organic Halogen and Developmental Toxicity of Chlorinated Drinking Water Might Be Attributed to Aromatic Halogenated DBPs? *Environ. Sci. Technol.* **2021**, *55* (9), 5906−5916.
(74) Lu, Y.; Song, Z.-M.; Wang, C.; Liang, J.-K.; Hu, Q.; Wu, Q.-Y. Nontargeted Identification of Chlorinated Disinfection Byproducts Formed from Natural Organic Matter Using Orbitrap Mass Spectrometry and a Halogen Extraction Code. *J. Hazard. Mater.* **2021**, *416*, 126198.
(75) Richardson, S.; Plewa, M.; Wagner, E.; Schoeny, R.; Demarini, D. Occurrence, Genotoxicity, and Carcinogenicity of Regulated and Emerging Disinfection by-Products in Drinking Water: A Review and Roadmap for Research. *Mutat. Res. Rev. Mutat.* **2007**, *636* (1−3), 178−242.

https://doi.org/10.1021/acs.est.2c06381
Environ. Sci. Technol. XXXX, XXX, XXX−XXX